2005

Boundary shear stress in spatially varied flow with increasing discharge

M. H. Khiadani
Isfahn University of Medical Sciences, Iran

S. Beecham
University of Technology Sydney

J. Kandasamy
Department of Infrastructure, Planning & Natural Resources, NSW

Muttucumaru Sivakumar
University of Wollongong, siva@uow.edu.au

Publication Details

This article was originally published as: Khiadani, MH, Beecham, S, Kandasamy, J & Sivakumar, S, Boundary Shear Stress in Spatially Varied Flow with Increasing Discharge, Journal of Hydraulic Engineering, 2005, 131(8), 705-714. Copyright 2005 American Society of Civil Engineers. Journal information available here.

Boundary Shear Stress in Spatially Varied Flow with Increasing Discharge

Mehdi H. Khiadani[1]; Simon Beecham[2]; Jaya Kandasamy[3]; and Siva Sivakumar[4]

Abstract: The distribution of the wall shear stress on the bed and sidewalls of an open channel receiving lateral inflow was obtained from experimental measurements of the distribution of the velocity in the viscous sublayer using a laser doppler velocimeter. The experiments were conducted in a 0.4 m wide by 7.5 m long flume. Lateral inflow was provided into the channel from above via sets of nozzles positioned toward the downstream end of the flume. Lateral inflow was provided over a length of 1.9 m. The results indicate that the local boundary shear stresses are significantly influenced by lateral inflow. The significant variation occurs near and around the region where the lateral inflow enters the channel. At various measurement positions along the lateral inflow zone, mean boundary, mean wall, and mean bed shear stresses were obtained and compared. The results indicate that the mean boundary shear stresses increase from the upstream to the downstream ends of the lateral inflow zone. The results also indicate that the mean bed shear stress is always greater than the mean wall shear stress, which are approximately 30–60% of the mean bed shear stress. The friction factor in the Darcy–Weisbach equation was obtained from both the mean boundary shear stress and from the equation describing the water surface elevation in an open channel receiving lateral inflow (equation for spatially varied flow with increasing discharge). The results indicate that the estimated friction factors from the latter approach are significantly larger. Also, the estimated friction factors from both approaches are higher than the values predicted from the Blasius equation which describes the friction factor for wide uniform open channel flows. They were also higher than values predicted from the Keulegan equation, which is an empirically derived equation for flow in roof drainage gutters. The study highlights the deficiencies in the existing equations used to predict friction factors for spatially varied flow and that further research is required to explore the distribution of boundary shear stress in an open channel receiving lateral inflow.

DOI: 10.1061/(ASCE)0733-9429(2005)131:8(705)

CE Database subject headings: Friction factor; Wall friction; Friction coefficient; Shear walls; Open channels; Velocity distribution.

Introduction

This paper describes an experimental investigation into the distribution of wall shear stress on the bed and sidewalls of a channel receiving lateral inflow. In this type of flow the discharge continuously increases in the longitudinal direction and this is termed spatially varied open channel flow with increasing discharge. This occurs in various situations. Examples include flow inside channel spillways and side weirs, in roof drainage gutters, in channels around sedimentation tanks, in wash water gutters at treatment plants, in irrigation distribution systems, and in overland flow under rainfall. The theoretical formulation and experimental investigation of spatially varied flow with increasing discharge have been of interest to many researchers in the fields of hydraulics, hydrology, and soil science. Theoretical studies in this area have been mainly based on a one-dimensional analysis of spatially varied flow. In this approach, the principle of linear momentum together with the equation of continuity have been used to develop an equation for variation of the water surface elevation (Hinds 1926; Faver 1933; Beij 1934; Camp 1940; Keulegan 1952; Li 1955; Yen and Wenzel 1970; Yen et al. 1972; Hager 1983, 1985).

Considering the conservation of mass and momentum, and assuming that the pressure is hydrostatic over the cross section of the channel, the following equation for steady spatially varied flow with increasing discharge can be obtained, Yen and Wenzel (1970):

$$\frac{dh}{dx} = \frac{S_0 - \frac{\tau_{0x}}{\gamma R} + \frac{q}{gA}(U_L \cos\phi - 2U)}{1 - \mathrm{F}^2} \tag{1}$$

where A=cross-sectional area; h=flow depth; F=Froude number; U=average velocity over the channel cross section; U_L=lateral inflow velocity at the water surface in the channel that may have an angle ϕ relative to the x direction (note: in this study lateral inflow always entered normal to the channel bed); q=lateral inflow rate per meter length; S_0=channel slope; R=hydraulic radius; g=acceleration due to gravity; γ=specific weight of the fluid; and τ_{0x}=boundary shear stress in the x direction.

The traditional approach in open channel or pipe flow analysis is to evaluate the average boundary shear stress using Manning's equation or the Darcy–Weisbach equation. Strictly speaking, these equations are for uniform open channel or pipe flows. Using these equations for other cases may require adjusting the Man-

[1] Assistant Professor, Isfahn Univ. of Medical Sciences, Isfahn, Iran.
[2] Associate Lecturer, Univ. of Technology, Sydney, NSW 2007, Australia.
[3] Floodplain Specialist, Dept. of Infrastructure, Planning and Natural Resources, NSW, Australia.
[4] Associate Professor, Univ. of Wollongong, Wollongong, NSW 2522, Australia.

Note. Discussion open until January 1, 2006. Separate discussions must be submitted for individual papers. To extend the closing date by one month, a written request must be filed with the ASCE Managing Editor. The manuscript for this paper was submitted for review and possible publication on April 18, 2003; approved on August 18, 2004. This paper is part of the ***Journal of Hydraulic Engineering***, Vol. 131, No. 8, August 1, 2005. ©ASCE, ISSN 0733-9429/2005/8-705–714/$25.00.

ning's "*n*" and the Darcy's friction coefficients. Moreover, an estimation of the local boundary shear stress cannot be obtained using this approach. The purpose of this study is to measure the local boundary shear stresses, the average boundary shear stresses, and consequently the friction factor for an open channel receiving lateral inflow.

For spatially varied flow with increasing discharge, Keulegan (1952) estimated the friction factor in the Darcy–Weisbach equation using Beij's (1934) data. He estimated the friction factor from the measured water surface profiles by backsubstitution in the one-dimensional equation for spatially varied flow. Keulegan (1952) assumed that the velocity distribution is uniform and the distribution of pressure is hydrostatic. In addition, the longitudinal momentum due to the lateral inflow was ignored. The estimated friction factors were very large compared to the values produced from the Blasius equation for wide uniform open channel flows. Estimating the friction factor by this approach requires prior knowledge of the water surface elevation in the channel. Although this approach may be useful for practical purposes questions do arise. First, can Keulegan's estimated friction factors be used for flow situations other than those tested by Beij? Second, do the estimated friction factors truly represent the friction at the channel boundary? Third, what is the distribution of the local boundary shear stresses? These questions could not readily be answered in the past because no attempt has been made to conduct measurements of the boundary shear stresses in the case of spatially varied flow with increasing discharge.

This paper presents measurements of the local boundary shear stresses in an open channel receiving vertical inflow along the length of the channel. The average boundary shear stresses are first determined and this is followed by an estimation of the friction factors. The friction factors were estimated using a similar approach to Keulegan (1952), from the equation for spatially varied flow with increasing discharge. The results were compared with the Blasius equation for wide uniform open channel flows and with the equation obtained by Keulegan (1952) for flow in roof drainage gutters.

Determination of Boundary Shear Stress

Various techniques have been developed to determine the boundary shear stress in open channel flow. Examples include direct measurement, momentum balance evaluation, the use of liquid tracers and the assessment of wall similarity. A comprehensive review can be found in Brown and Joubert (1967), Winter (1977), Hanratty and Campbell (1983), Knight and Patel (1985), Haritonidis (1989), Farnhoiz et al. (1996), and Ackerman and Hoover (2001). In this study, the local boundary shear stresses were determined from an assumed linear distribution of velocity in the viscous sublayer using a laser doppler velocimeter (LDV). Mazumder et al. (1981), Kirgoz (1989), Ching et al. (1995), Durst et al. (1996), and Nezu and Rodi (1986) are among those who used LDV to measure the boundary shear stress from the velocity gradient inside the viscous sublayer.

From the linear distribution of the velocity close to the boundary within the viscous sublayer, the local boundary shear stress can be obtained as follows:

$$\tau_{0x} = \mu \frac{du}{dy} \tag{2}$$

where μ=dynamic viscosity; y=distance from the channel bed; u =mean longitudinal local velocity; and τ_{0x}=local boundary shear stress.

In dimensionless wall coordinates, the distribution of velocity in the viscous sublayer can be written as follows:

$$U^+ = Y^+ \tag{3}$$

where $Y^+ = yu_*/\nu$; and $U^+ = u/u*$ with $u* = (\tau_{0x}/\rho)^{1/2}$ with ρ being the mass density of the fluid. This equation may be valid up to $Y^+ < 10$ (Mazumder et al. 1981).

The average boundary shear stress can be estimated as follows:

$$\overline{\tau}_{0x} = \frac{1}{P}\int_0^P \tau_{0x} dP \cong \frac{1}{P}\sum_{i=1}^{N} \tau_{0x}\Delta P \tag{4}$$

where P=wetted perimeter of the boundary; and N=number of increments.

Dimensional analysis together with the Darcy–Weisbach formula provide a relationship between the friction factor f and the boundary shear stress. This relationship can be described as follows:

$$f = \frac{8\overline{\tau}_{0x}}{\rho U^2} \tag{5}$$

In addition to the previous method, the friction factors were also estimated from the one-dimensional equation for spatially varied flow with increasing discharge [Eq. (1)], using the measured water surface slope. Eq. (1) can be rearranged to express the friction factor:

$$f = \frac{8gR}{U^2}\left[S_0 + \frac{q}{gA}(U_L \cos\phi - 2U) - (1 - \mathrm{F}^2)\frac{dh}{dx}\right] \tag{6}$$

Experimental Arrangement

Figs. 1 and 2 show the longitudinal and plan view of the flume and lateral inflow devices. The experimental equipment used in this study included a flume and circulating system, lateral inflow generator, a LDV, and a traversing system. The experimental arrangement is described in the following.

Flume and Lateral Inflow Devices

The flume was 0.4 m wide by 7.5 m long. The side walls were 0.20 m high. The flume was made of 10-mm-thick perspex. A fine screen was mounted at the entrance to the flume to ensure an evenly distributed flow entered the channel. An electromagnetic flux flowmeter was used to measure the flow rate entering the flume.

The lateral inflow was provided by 16 nozzles, hoses, a supporting frame, 8 flowmeters, and a pump. An even flow distribution was achieved through the nozzles with a maximum estimated error of ±4.0% (Khiadani 2000).

Laser Doppler Velocimeter System

The measurements were carried out using a two-color fiber-optic LDV with an IFA 750 signal processor (digital burst correlator) and processing software. The LDV system was operated in backscattering mode and could detect flow reversal. The following

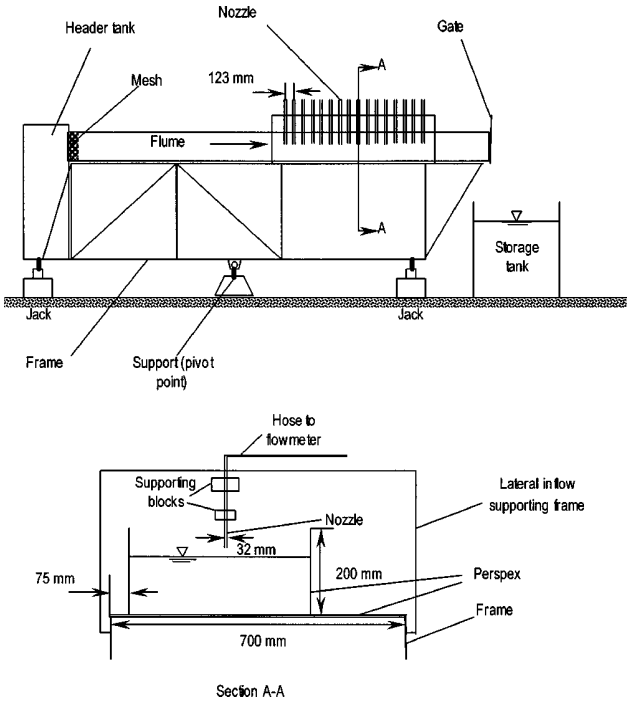

Fig. 1. Flume and lateral inflow devices

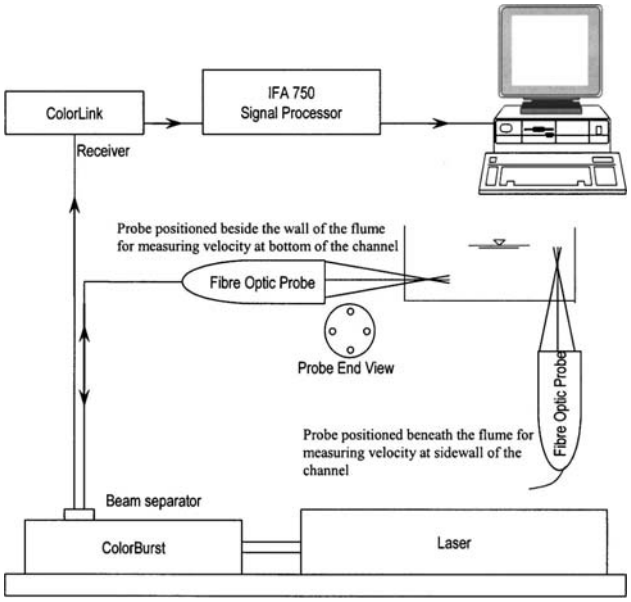

Fig. 3. Laser doppler system components

processor setup was chosen for the reported measurements: random mode with time stamp, burst transit time weighting, processor control target efficiency of 55%, and medium signal-to-noise ratio. Fig. 3 shows different components of the LDV system. The optical specifications of the LDV are presented in Table 1.

The fiber-optic probe was mounted on a mechanical traverse system, which was capable of accurately positioning the fiber-optic probe over the length, width, and height of the flume. In normal operation, a positioning accuracy of ±0.5 mm was achievable. Fine placement of the probe was achieved using a dial gauge with an accuracy of ±0.005 mm. During the testing program the flow was seeded with hollow glass spheres with an average particle size of 10 μm to increase the data collection rate for the LDV. For each measurement around 5,000 data points were collected over a period of about 5 mins. The data rate varied from 10 to 50Hz depending on the location of measurements. For data collected at each position signal bursts were monitored using an oscilloscope. In addition during data postprocessing checks on the data were undertaken to make sure data were not noise contaminated. Further details of the experimental setup are given in Khiadani (2000).

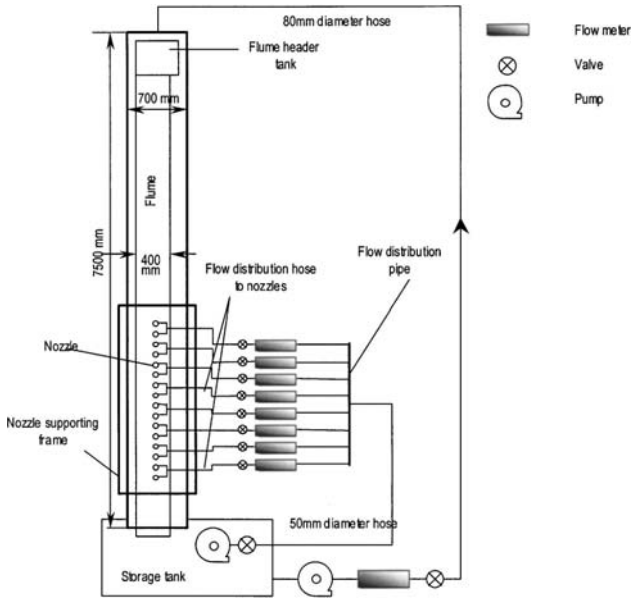

Fig. 2. Plan view of flume and lateral inflow devices

Uniform Flow Tests

To ensure that the flume and the measuring instruments had been set up accurately two velocity profiles were measured in the center of the channel, 4,575 mm from the upstream end of the channel. The discharge in the flume was constant with no lateral inflow. The flow conditions under which these tests were conducted are given in Table 2.

Table 1. Optical Specifications of Laser Doppler Velocimeter System

	Laser color	
Optical characteristics	Green	Blue
Number of laser beams	2	2
Wavelength (nm)	514.5	488.0
Probe beam spacing (mm)	50	50
Focal length in air (mm)	349.7	349.7
Beam diameter (mm)	2.82	2.82
Beam crossing half angle (deg)	3.95	3.95
Measurement volume diameter (μm)	90.5	85.8
Measurement volume length (mm)	1.31	1.24
Fringe spacing (μm)	3.73	3.54
Number of fringes	24.2	24.2

Table 2. Flow Condition under No Lateral Inflow Conditions

Profile	Q(L/s)	Channel width, B (m)	Flow depth, h (m)	Slope (%)	Mean channel velocity, U(m/s)	Froude (F)	Reynolds (R)	Shear velocity, $u*$(m/s)
1	5.0	0.40	0.022	0.30	0.57	1.22	11,200	0.032
2	10.0	0.40	0.031	0.30	0.81	1.46	21,500	0.040

Spatially Varied Flow Tests

The spatially varied flow experiments included two data subsets, termed Series AN and BN. Table 3 indicates the flow conditions for each series. A base flow of 5 L/s was provided in the flume for both Series AN and BN. The base flow is the discharge in the flume upstream of the zone of lateral inflow. The nozzle flow rate from Series AN to BN was increased by 32%.

For each series, the water surface profile was measured at 100 mm intervals from the upstream to the downstream ends of the lateral inflow zone using a needle depth gauge with a reading accuracy of ±0.05 mm. The flow depth for each series was measured about 70 mm away from the centerline of the flume to avoid any flow disturbance effects due to the nozzles discharging along the centerline. The flow depths across the flume width were also measured at selected locations to measure variation of depth across the flume width. However, no measurable difference was recorded.

The locations of cross sections where local boundary shear stresses were obtained are shown as dotted lines in Fig. 4. Fig. 5 shows a three-dimensional view of the cross sections and the locations where the boundary shear stresses were obtained. Measurements were taken for half of the cross section because the flow conditions were symmetrical across the centerline of the flume. The nozzles discharged normal to the flume floor and along the flume centerline. The symmetrical flow conditions were verified by measuring the velocity profiles, u, at three pairs of symmetrical positions, with respect to the channel centerline, at $x=4{,}950$ mm. The nozzle flow rates and base flow were 0.25 and 5 L/s, respectively. The maximum asymmetry was found to be 6.0% of the nozzle average velocity, V_n.

Within the lateral inflow zone, between $x=4{,}590$ and 4,750 mm, except for the cross sections located between $x=5{,}501.5$ and 5,747.5 mm, the measurements were taken in the middle of two consecutive nozzles. For each cross section, the local boundary shear stresses at the bed were measured across half of the flume cross section at eight spanwise positions, $2z/B=0$, 0.125, 0.25, 0.375, 0.5, 0.625, 0.75, and 0.825. At the flume sidewall the measurements were taken at 10 mm intervals beginning at the bed. For the cross section at $x=7{,}050$ mm, no measurement was performed at the channel sidewall. This was due to the blockage of the laser beams by the flume-supporting frame. To explore the distribution of boundary shear stresses between two consecutive nozzles, the measurements between $x=5{,}501.5$ and 5,747.5 mm were performed at 20 mm intervals starting from $x=5{,}501.5$ mm. For these cross sections, the local boundary shear stresses at the bed were measured across the width of the flume at three spanwise locations $2z/B=0.0$, 0.375, and 0.75. No measurement was taken at the flume sidewall for these sets of experiments.

For each measurement position, the longitudinal velocity, u, was measured at 0.05, 0.075, 0.1, 0.125, 0.15, and 0.20 mm from the boundary. The velocities at the channel bed were measured by placing the laser probe beside the sidewall (guiding the laser beam from sidewall). On the other hand the laser probe was placed under the flume for measuring the velocity at the sidewall (see Fig. 3). This arrangement enabled measurements very close to the channel bed. For measurements in the viscous sublayer only the green laser light was used. The boundary shear stress was estimated by fitting a least squares straight line to the near wall data. For a limited number of locations, one or two measured data points close to the boundary were excluded from the least squares procedure. It was suspected that these outlier measurements were due to noise effects.

Table 3. Summary of Flow Conditions for Series AN and BN

Run	Flume base flow (L/s)	Nozzle flow (L/s per nozzle)	Nozzle internal diameter (mm)	Nozzle average velocity ($V_n=q\hat{n}/A\hat{n}$)(m/s)	Flume slope (%)
AN	5	0.25	28	0.41	0.30
BN	5	0.33	28	0.54	0.30

Results

Uniform Flow Results

Table 2 shows the experimental configurations for conditions where there is no lateral inflow to the channel. The shear velocity, u_*, has been estimated from the velocity profile within the viscous sublayer. The shear velocity, $u*$, was also estimated from a best fit of the log law within the inertial sublayer ($y/h<0.2$). The difference between the two approaches was within 2%. The velocity profiles are plotted in Fig. 6 in wall coordinate scales of U^+ and Y^+. Also shown is the equation for the distribution of velocity in a two-dimensional uniform open channel flow suggested by Nezu and Rodi (1986). There is a close agreement between the results of this study with the equation by Nezu and Rodi as shown in Fig. 6. This implies that the flume and instrument were accurately set up and suitable for experimentation with lateral inflow.

Spatially Varied Flow Results

Water surface profiles for the spatially varied flow tests are presented in Fig. 7. Table 4 presents the mean flow conditions at various locations for each profile. Velocity profiles measured within the viscous sublayer (to obtain the local boundary shear stress) are presented in Khiadani (2000). Fig. 8 shows typical measured velocity profiles at cross section $x=5{,}993.5$ mm under conditions in which the flow rate, qn, from each nozzle was 0.25 L/s.

For Series AN and BN, Fig. 9 illustrates the distribution of the normalized bed shear stress, $\tau_b/\overline{\tau_{0x}}$, and the normalized wall shear stress, $\tau_w/\overline{\tau_{0x}}$, that were measured upstream, within and down-

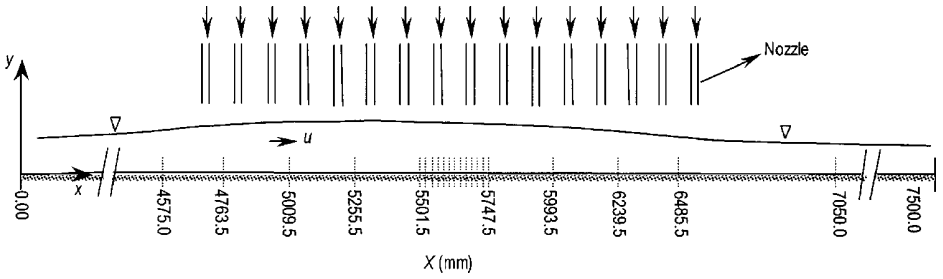

Fig. 4. Longitudinal measurement locations along the flume

stream of the lateral inflow zone. $\overline{\tau_{0x}}$ is the average shear stress over the wetted perimeter. The normalized bed shear stress, is plotted against the normalized transverse distance, $2z/B$, and the normalized wall shear stress is plotted against y/h. Fig. 9 shows that at $x=4{,}575$ and 7,050 mm, the variation of the normalized bed shear stress in the transverse direction is not significant in comparison with other sections. The cross section at $x=4{,}575$ mm corresponds to a distance 127 mm upstream of the center of the first nozzle and the cross section at $x=7{,}050$ mm corresponds to a distance 502 mm downstream of the lateral inflow zone (from the center of the most downstream nozzle). Note that even when the flow out of each nozzle has increased by 32%, there is no sign of influence of the lateral inflow on the normalized bed shear stress at these locations.

For other cross sections shown in Fig. 9, the normalized bed shear stress, $\tau_b/\overline{\tau_{0x}}$, decays with increasing values of $2z/B$. In other words, for a particular cross section in which the measurements are conducted at the center of two consecutive nozzles, the normalized bed shear stress has a maximum value at the channel centerline, then it reduces toward the channel wall. The transverse variation of the normalized bed shear stress is notable up to $2z/B=0.50$. However, further downstream in the channel the transverse variation of $\tau_b/\overline{\tau}0x$ is less pronounced. To see this effect more clearly, for each transverse location, the longitudinal variation of $\tau_b/\overline{\tau_{0x}}$ is plotted in Figs. 10 and 11 for Series AN and BN, respectively. As can be seen from these plots, for $2z/B=0.0$, 0.125, and 0.25 the normalized bed shear stress increases as the lateral inflow zone is approached, then decreases (overall) in the downstream direction. For $2z/B=0.375$ and $2z/B=0.50$, the normalized bed shear stress, $\tau_b/\overline{\tau_{0x}}$, does not vary significantly along the length of the lateral inflow. One may expect the normalized bed shear stress to also increase due to the increase of mean velocity in the downstream direction. However, for $2z/B=0.625$, 0.75, and 0.875, the normalized boundary shear stress, $\tau_b/\overline{\tau_{0x}}$ increases slightly in the downstream direction. Such behavior may be due to the influence of lateral inflow at the various measurement positions. Again, a comparison of Series AN and BN indicates that an increase of lateral inflow by 32% has not significantly influenced the distribution of normalized bed shear stresses.

The bed shear stresses were also measured in detail between two consecutive nozzles from $x=5{,}501.5$ to 5,747.5 mm. As pointed out earlier, measurements were conducted at $2z/B=0.0$, 0.375, and 0.75 in the transverse direction. The measured bed shear stresses between these nozzle positions are given in Fig. 12. It can be seen that at the channel centerline, $2z/B=0.0$, the measured bed shear stresses start to decrease as we move toward the nozzle. The stresses become negative slightly upstream of the nozzle axis. Then they increase to a maximum value downstream of the nozzle. A similar pattern can be seen for the next downstream nozzle. The negative values of the bed shear stresses in these regions are an indication of reverse flow. This implies that

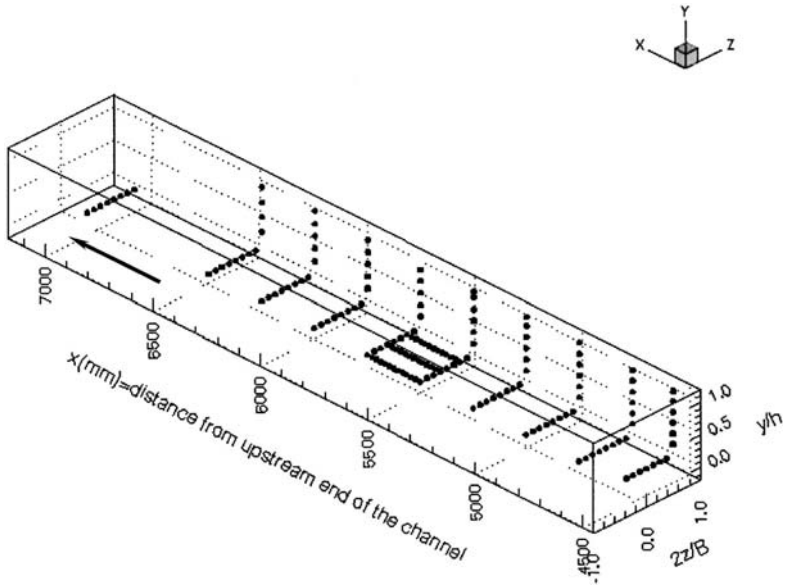

Fig. 5. Measurement locations at various sections

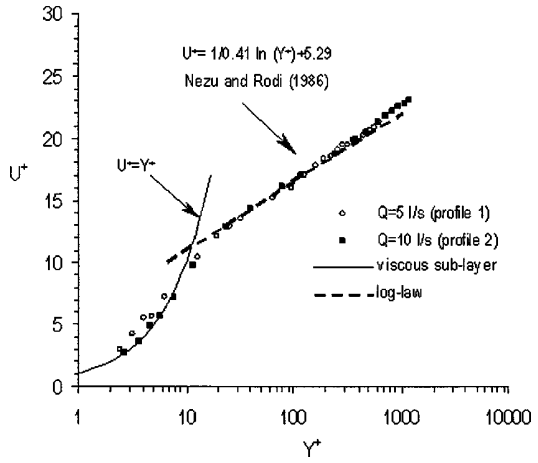

Fig. 6. Dimensionless plot of measurements in channel receiving no lateral inflow

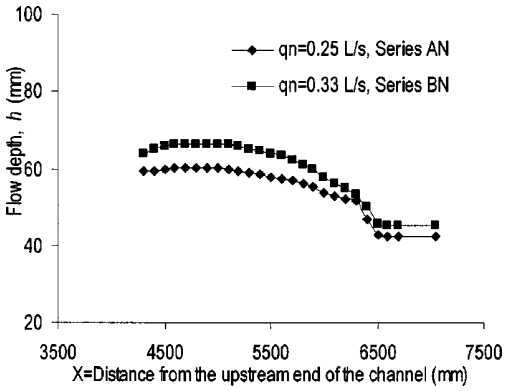

Fig. 7. Water surface levels for Series AN and BN

the nozzle flow impinges on the channel floor, and then spreads in all directions in the floor region. At the stagnation point the bed shear stress becomes zero. Due to the main channel flow the nozzle flow deflects. As a result, the impingement region moves downstream of the jet where the maximum bed shear stress occurs.

Fig. 12 shows that for transverse locations $2z/B=0.375$ and $2z/B=0.75$ there are no significant variations in the measured bed shear stresses of the type observed for $2z/B=0.0$. This implies that at these locations the effect of the lateral inflow on the bed shear stress is not as strong as at $2z/B=0.0$, where the nozzle flows enter the channel.

It is also interesting to note that there is no significant difference in the measured bed shear stresses for the two different lateral inflow rates that were tested. This may be due to the small difference between the relative magnitude of the nozzle velocity, at the water surface, compared to the channel mean velocity, U_L/U, as well as the small variation of flow depth. As an example, at $x=5{,}501.5$ mm the velocity ratios U_L/U for $q_n=0.25$ and 0.33 L/s are 2.65 and 2.72, respectively. The difference is only 2.6%. At this location, due to the increase in flow rate, the flow depth has increased by around 10%. Due to the small difference in velocity ratio the influence of this parameter cannot be determined, but this may be an area of further investigation.

Distribution of Mean Boundary Shear Stress

The distribution of the mean boundary shear stress in open channel flows, and in particular in spatially varied flow, is very impor-

Table 4. Details of Experimental Conditions for Series AN and BN

x (mm)	h (mm)	A (m^2)	R (m)	Q (m^3/s)	U (m/s)	R	F
AN-test ($qn=0.25$ L/s)							
4575.0	60.30	0.0241	0.0463	0.0050	0.207	9,600	0.27
4763.5	60.35	0.0241	0.0464	0.0053	0.217	10,000	0.28
5009.5	60.15	0.0241	0.0462	0.0058	0.239	11,000	0.31
5255.5	59.15	0.0237	0.0456	0.0063	0.264	12,000	0.35
5501.5	57.75	0.0231	0.0448	0.0068	0.292	13,000	0.39
5747.5	56.67	0.0227	0.0442	0.0073	0.320	14,100	0.43
5993.5	53.88	0.0216	0.0424	0.0078	0.360	15,200	0.49
6239.5	51.80	0.0207	0.0411	0.0083	0.398	16,300	0.56
6486.5	43.30	0.0173	0.0356	0.0088	0.505	17,900	0.78
7050.0	42.50	0.0170	0.0351	0.0090	0.529	18,500	0.82
BN-test ($qn=0.33$ L/s)							
4575.0	66.19	0.02648	0.04973	0.0050	0.189	9,300	0.23
4763.5	66.30	0.02652	0.04979	0.0053	0.201	10,000	0.25
5009.5	66.30	0.02652	0.04979	0.0060	0.226	11,200	0.28
5255.5	65.35	0.02614	0.04926	0.0067	0.254	12,500	0.32
5501.5	63.90	0.02556	0.04843	0.0073	0.286	13,800	0.36
5747.5	61.62	0.02465	0.04711	0.0080	0.323	15,200	0.42
5993.5	57.87	0.02315	0.04488	0.0086	0.373	16,700	0.49
6239.5	54.40	0.02176	0.04277	0.0093	0.427	18,200	0.58
6486.5	46.30	0.01852	0.03760	0.0100	0.537	20,100	0.80
7050.0	45.00	0.01800	0.03673	0.0103	0.571	20,900	0.86

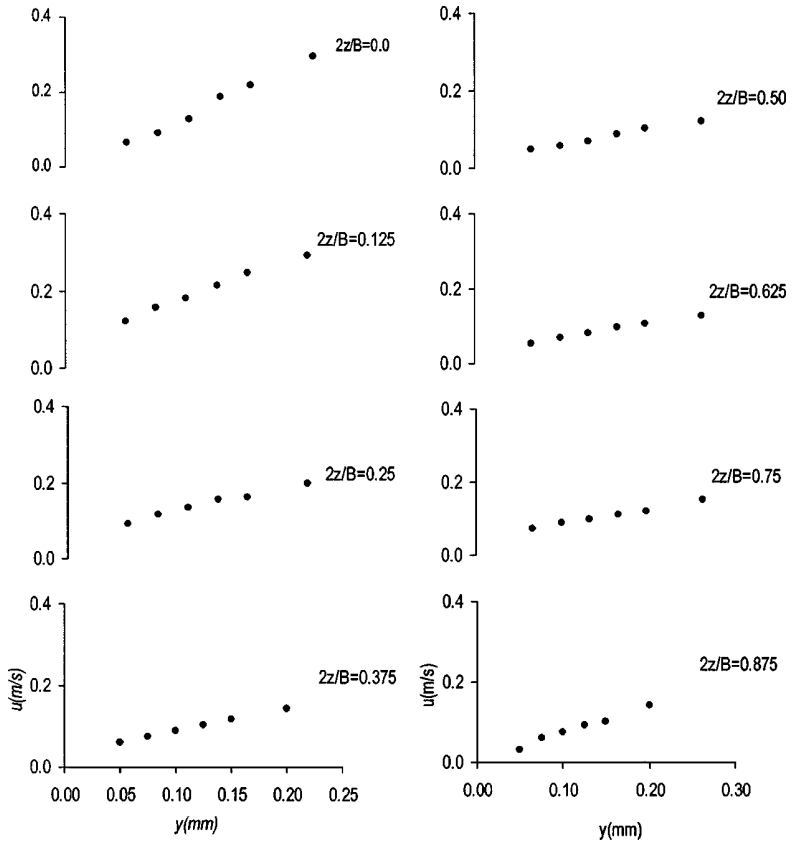

Fig. 8. Measured velocity profiles within the viscous sublayer at $x=5993.5$ mm for $q_n=0.25$ l/s.

tant in the determination of flow behavior. For the one-dimensional analysis of spatially varied flow, it is of interest to solve the momentum equation for the water surface slope. For such analysis, the friction slope, $S_f=\overline{\tau}_{0x}/\gamma R$, which directly relates to the average boundary shear stress, needs to be evaluated.

For Series AN and BN the mean boundary shear stresses for the channel bed, $\overline{\tau}_b$, the channel wall, $\overline{\tau}_w$, and the channel wetted perimeter, $\overline{\tau}_{0x}$, are estimated and plotted in Figs. 13 and 14.

In these figures the mean wall shear stress, $\overline{\tau}_w$, continuously increases along the lateral inflow zone. This may be explained by the fact that the mean velocity of the flow increases, due to the lateral inflow, in the downstream direction of the channel. It can also be seen that the mean bed shear stress, $\overline{\tau}_b$, increases rapidly as flow approaches the lateral inflow zone. This increase in $\overline{\tau}_b$ continues through the lateral inflow zone until it reaches a maximum at the downstream end of the inflow zone.

A comparison of the mean wall and the mean bed shear stresses using Series AN and BN in Figs. 13 and 14 indicates that the mean bed shear stresses are considerably higher. To give a quantitative indication of the difference, 50% error bars for the mean bed shear stresses, $\overline{\tau}_b$, are plotted. The bed shear stress, $\overline{\tau}_b$, is 30–60% greater than $\overline{\tau}_w$. A direct comparison with Knight and Patel (1985) is not possible as their experiments were for uniform open channel flow conditions in channels that were significantly different from the type used in this study. However, Knight and Patel (1985) found the relative magnitude of the bed to the wall shear stress depends on the channel aspect ratio, B/h and as B/h increases, $\overline{\tau}_b/\overline{\tau}_w$ increases. Their results indicated that $\overline{\tau}_b$ is 1.5% (for $B/h\approx 1$) to 51% (for $B/h\approx 10$) greater than $\overline{\tau}_w$. For the tests conducted in this study the ratio of the channel width to depth, B/h, varied from 6 to 9.

Darcy–Weisbach Friction Factor

For the spatially varied flow experiments conducted in this study, the estimated friction factors from the velocity measurements close to the channel boundary are plotted against the Reynolds number in Fig. 15. As a guide, estimated friction factors from the equation for spatially varied flow with increasing discharge [Eq. (6)] are also plotted. The lines representing the Blasius and the Keulegan equations are also given. The results indicate that along the lateral inflow zone the friction factor decreases as the Reynolds number increases.

The Blasius equation gives reasonable predictions for channels that do not receive lateral inflow. It also gives reasonable predictions in the portions of the channel upstream and downstream of zones of lateral inflow. The Blasius equation was derived from experiments in wide rectangular channels with uniform flow.

In the lateral inflow zone for channels receiving lateral inflow, the friction factors are significantly higher than the Blasius equation and even the Keulegan equations. Note the Keulegan equation was derived from Beij's experiments in a narrow channel with a varying lateral inflow rate. Beij carried out his tests in a 9.63 m long by 0.152 m wide rectangular cross-section channel. The channel slopes were $S_0=3.12$, 2.08, 1.04, and 0.52%. The

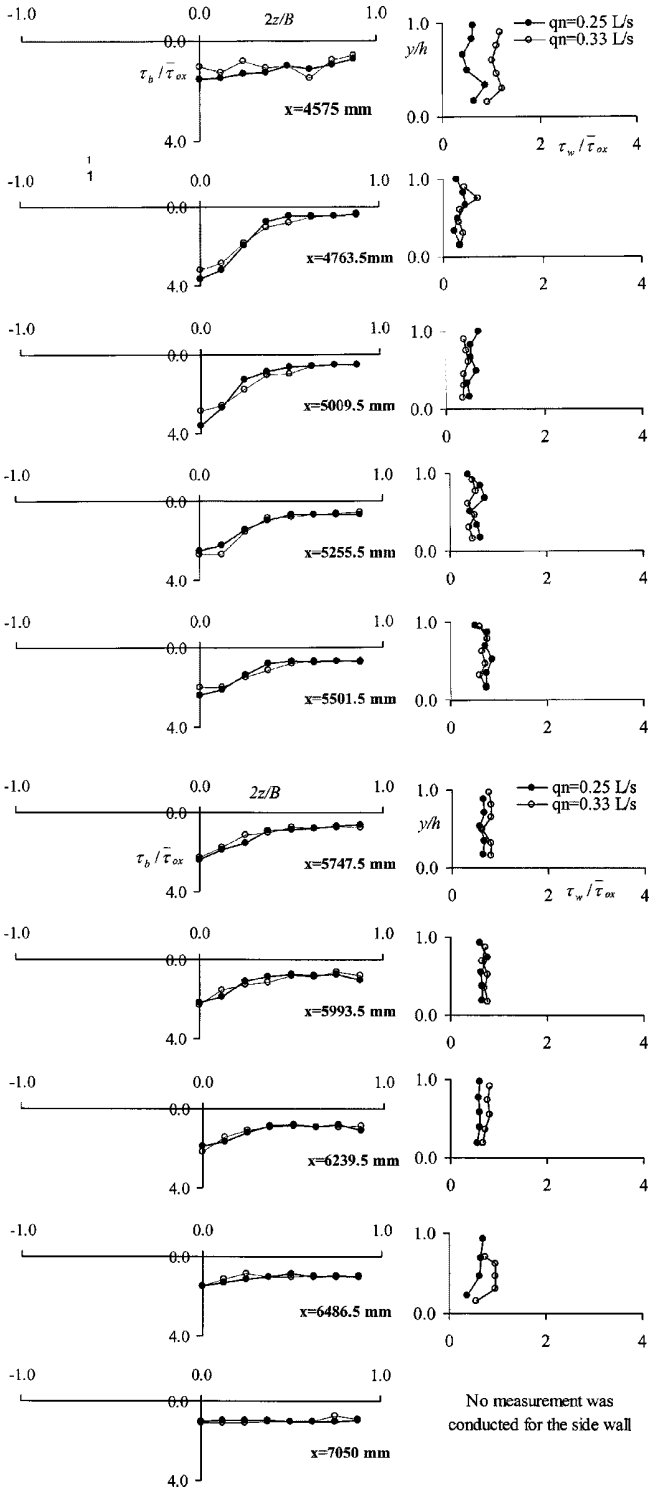

Fig. 9. Local bed shear stresses for Series AN and BN

lateral inflows were varied for each slope configuration. In Beij's experiments, the maximum lateral inflow rate was approximately 0.6 L/s/m. In this study, however, the corresponding lateral inflow rates for $q_n=0.25$ L/s and $q_n=0.33$ L/s were almost 2.1 and 2.8 L/s/m, respectively. The much larger lateral inflow partly accounts for why the friction factor derived from the experimental

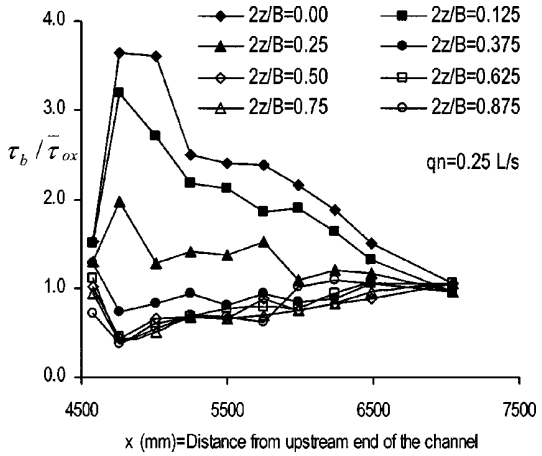

Fig. 10. Longitudinal variation of local bed shear stresses for $q_n=0.25$ L/s (Series AN)

data is much larger than the Keulegan equation. The Keulegan equation is

$$f=\frac{320}{\mathrm{R}} \tag{7}$$

The Blasius equation is

$$f=\frac{0.223}{R^{0.25}} \tag{8}$$

The estimated friction factors from the equation for spatially varied flow with increasing discharge [Eq. (6)] are considerably larger than those estimated from velocity measurements. This may be due to the assumptions required in the derivation of the one-dimensional equation for spatially varied flow with increasing discharge. In Eq. (6) it is assumed that the distribution of velocity is uniform, the pressure distribution is hydrostatic, the secondary flow influence is not significant, and the effects of turbulence can be ignored. The estimated friction factors may have compensated for the assumptions that have been made in the derivation of the spatially varied flow equation [Eq. (6)]. Note that estimating the friction factor from the spatially varied flow equation requires knowledge of the water surface profile. Although this is useful for research purposes, it has limited application as a design tool. It is intended to further investigate the nature of this

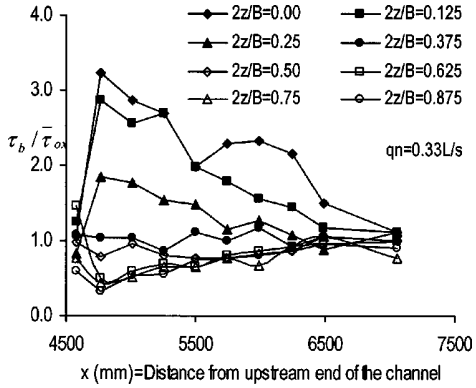

Fig. 11. Longitudinal variation of local bed shear stress for $q_n=0.33$ L/s (Series BN)

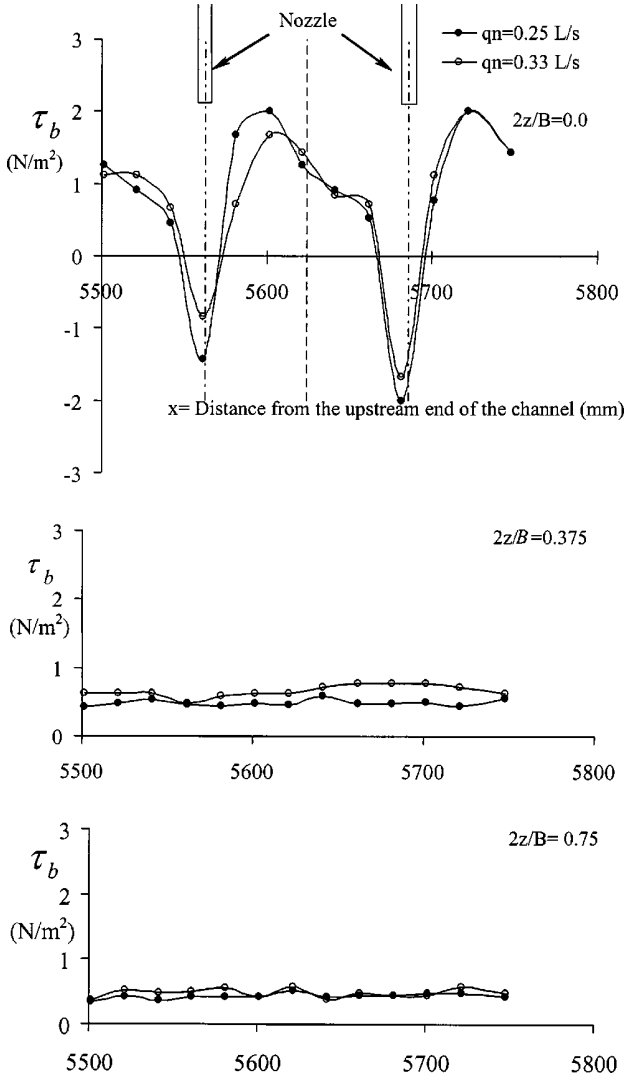

Fig. 12. Distribution of local boundary shear stresses between two consecutive nozzles

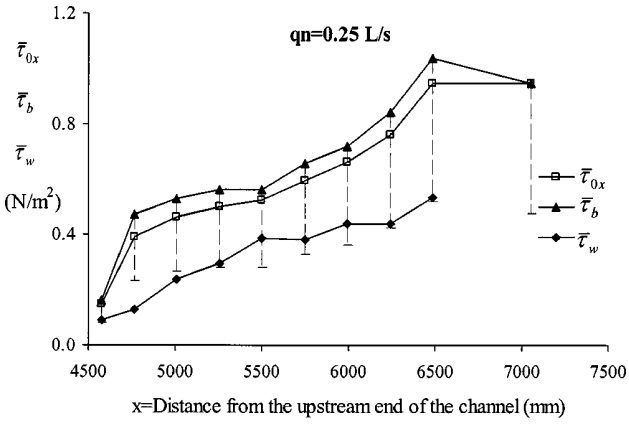

Fig. 13. Average boundary shear stresses (q_n=0.25 L/s, Series AN)

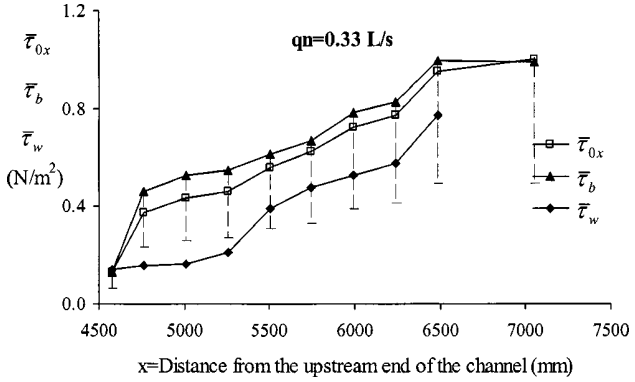

Fig. 14. Average boundary shear stresses (q_n=0.33 L/s, Series BN)

type of spatially varied flow with the aim of providing a design methodology which enables an accurate prediction of friction factors without prior knowledge of the water surface profile.

Conclusions

The experimental data indicate that the local boundary shear stresses are significantly influenced by lateral inflow. The impact of lateral inflow on the distribution of boundary shear stress extends for some distance from where lateral flow joins the channel. Flow reversal is present where the nozzle flow impinges the channel bed.

The mean shear stresses, $\overline{\tau}_b$, $\overline{\tau}_w$, and $\overline{\tau}_{0x}$, increase along the lateral inflow zone with a minimum value at the upstream end and a maximum value at the downstream end. The mean bed shear stresses, $\overline{\tau}_b$, are always greater than the mean sidewall shear stresses, $\overline{\tau}_w$, which vary between approximately 30 and 60% of $\overline{\tau}_b$.

Logarithmic plots of the friction factor f versus the Reynolds number, R, indicate that the friction factor f depends on the Reynolds number, for the range $9{,}500 < R < 22{,}000$. The friction factor generally increases as the Reynolds number decreases. The Blasius equation gives reasonable predictions for channels that do not receive lateral inflow and in the portion of the channel upstream and downstream of the lateral inflow zone.

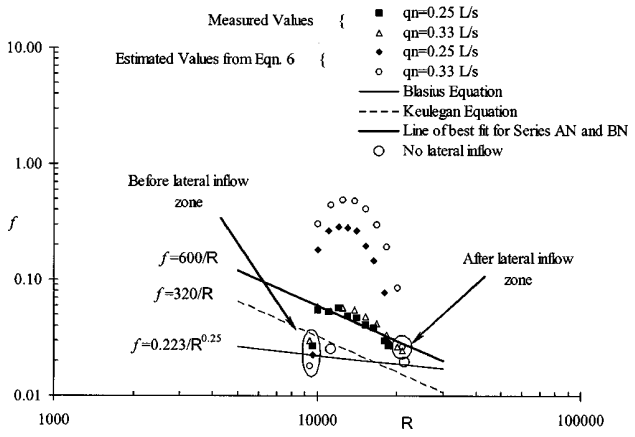

Fig. 15. Friction factor versus Reynolds number for Series AN and BN

The estimated friction factors derived from measurements collected in this study are considerably larger than the values estimated from the Keulegan equation. The estimation of friction factors from the equation for a one-dimensional equation for spatially varied flow [Eq. (6)] does not give the correct value. It was found that the estimated friction factors from the spatially varied flow equation were considerably larger than those estimated from velocity measurements. This is possibly due to various simplifications in deriving the spatially varied flow equation. This highlights the caution required when using these equations as they do not always describe friction loss in steady, spatially varied flow with increasing discharge.

Further research is required to explore both the distribution of boundary shear stress and the variation of friction factor over a wide range of flow conditions.

Notations

The following symbols are used in this paper:

A = cross-sectional area;
B = channel width at bed;
D = hydraulic depth defined as $D=A/T$;
d_m = measurement volume diameter corresponding to the laser beam crossing region;
F = Froude number;
f = Darcy–Weisbach resistance coefficient;
g = gravitational acceleration;
h = depth of flow section;
K = pressure correction factor;
l_m = measurement volume length corresponding to the laser beam crossing region;
n = Manning's roughness coefficient;
P = wetted perimeter;
p = pressure;
Q = main flow discharge;
q = lateral flow rate per unit length of channel;
q_n = flow rate for each nozzle;
R = Reynolds Number, defined as $\mathsf{R}=UR/\nu$;
R = hydraulic radius;
S_f = friction slope;
S_0 = channel bed slope;
U = mean longitudinal local velocity;
U_L = velocity of lateral inflow at the water surface;
u = mean longitudinal local velocity;
$u*$ = shear velocity;
V_n = mean velocity of the nozzles where the flow leave nozzle;
x,y,z = coordinates measured from origin;
α = U_L/U;
β = momentum coefficient;
γ = specific weight of the fluid;
θ = angle between channel bottom and horizontal plane;
μ = dynamic viscosity;
ν = kinematic viscosity;
ρ = mass density of the fluid;
τ_b = local streamwise bed shear stress;
τ_w = local streamwise side wall shear stress;
τ_{0x} = local streamwise boundary shear stress or wall shear stress on bed and side wall of the channel;
$\overline{\tau_b}$ = average bed shear stress;
$\overline{\tau_w}$ = average wall shear stress; and
$\overline{\tau_{0x}}$ = average boundary shear stress or wall shear stress on bed and side wall of the channel;
ϕ = angle between velocity vector of lateral flow and the direction of main channel flow.

References

Ackerman, J. D., and Hoover, T. (2001). "Measurement of local bed stress in streams using a Preston-static tube." *Limnol. Oceanogr.*, 46(8), 2080–2087.

Beij, K. H. (1934). "Flow in roof gutters." *J. Res. Natl. Bur. Stand.*, 12, 193–213.

Brown, G. L., and Joubert, P. N. (1967). "Measurement of skin friction in turbulent boundary layer with adverse pressure gradients." *J. Fluid Mech.*, 35(4), 737–757.

Camp, T. F. (1940). "Lateral spillway channels." *Trans. Am. Soc. Civ. Eng.*, 105, 606–617.

Ching, C. Y., Djenidi, L., and Antonia, R. A. (1995). "Low-Reynolds-number effect in a turbulent boundary layer." *Exp. Fluids*, 19(1), 61–68.

Durst, F., Kikura, H., Lekakis, I., Jovanovk, J., and Ye, Q. (1996). "Wall shear stress determination from near-wall mean velocity data in turbulent pipe and channel flows." *Exp. Fluids*, 20(6), 417–428.

Fernhoiz, H. H., Janke, G., Schober, M., Wagner, P. M., and Warnack, D. (1996). "New developments and applications of skin-friction measuring techniques." *Meas. Sci. Technol.*, 7(10), 1396–1409.

Faver, H. (1933). *Contribution a l'etude des courants liquides*, Rascher & Cie, Zurich, Switzerland (in French).

Hager, W. H., (1983). "Open channel hydraulics of flows with increasing discharge." *J. Hydraul. Res.*, 21(3), 177–193.

Hager, W. H. (1985). "Trapezoidal side-channel spillways." *Can. J. Civ. Eng.*, 12, 774–781.

Hanratty, T. J., and Campbell, J. A. (1983). "Measurements of wall shear stress." *Fluid mechanics measurements*, R. J. Goldstein, ed., Hemisphere, Washington, D.C., 559–615.

Haritonidis, J. H. (1989). "The measurement of wall shear stress." *Advances in fluid mechanics measurements*, M Gad-el-Hak, ed., Springer, Berlin, 229–261.

Hinds, J. (1926). "Side channel spillways." *Trans. Am. Soc. Civ. Eng.*, 89, 881–939.

Keulegan, G. H. (1952). "Determination of critical depth in spatially variable flow." *Proc., 2nd Midwestern Conf. on Fluid Mechanics, Bulletin 149*, Ohio State Univ., Engineering Experiment Station, Columbus, Ohio, 67–80.

Khiadani, M. H. (2000). "Hydraulics of spatially varied flow with increasing discharge." PhD Thesis, Univ. of Technology, Sydney, Australia.

Kirgoz, M. S. (1989). "Turbulent velocity profiles for smooth and rough open channel flow." *J. Hydraul. Eng.*, 115(11), 1543–1561.

Knight, D. W., and Patel, H. S. (1985). "Boundary shear in smooth rectangular ducts." *J. Hydraul. Div., Am. Soc. Civ. Eng.*, ASCE, 111(1), 29–47.

Li, W. H. (1955). "Open channels with nonuniform discharge." *Trans. Am. Soc. Civ. Eng.*, 120, 255–274.

Mazumder, M. K., Wanchoo, P. C., McLeod, P. C., Ballard, G. S., Mozumdar, S., and Caraballo, N. (1981). "Skin friction drag measurements by LDV." *J. Appl. Opt.*, 20(16), 2832–2837.

Nezu, I. and Rodi, W. (1986). "Open-channel flow measurements with a laser doppler anemometer." *J. Hydraul. Eng.*, 112(5), 335–355.

Winter, K. G. (1977). "An outline of the techniques available for the measurement of skin friction in turbulent boundary layers." *Prog. Aerosp. Sci.*, 18(1), 1–57.

Yen, B. C., and Wenzel, H. G. (1970). "Dynamic equations for steady spatially varied flow." *J. Hydraul. Div., Am. Soc. Civ. Eng.*, 96(3), 801–814.

Yen, B. C., Wenzel, H. G., and Yoon, N. Y. (1972). "Resistance coefficients for steady spatially varied flow." *J. Hydraul. Div., Am. Soc. Civ. Eng.*, 98(8), 1395–1410.